Altered Lumbar Spine Structure, Biochemistry, and Biomechanical Properties in a Canine Model of Mucopolysaccharidosis Type VII

Lachlan J. Smith,[1] John T. Martin,[1] Spencer E. Szczesny,[1] Katherine P. Ponder,[2] Mark E. Haskins,[3] Dawn M. Elliott[1]

[1]McKay Orthopaedic Research Laboratory, Department of Orthopedic Surgery, University of Pennsylvania, 424 Stemmler Hall, 36th and Hamilton Walk, Philadelphia, Pennsylvania 19104, [2]Department of Internal Medicine, School of Medicine, Washington University, St. Louis, Missouri, [3]Department of Pathobiology, School of Veterinary Medicine, University of Pennsylvania, Philadelphia, Pennsylvania

Received 26 May 2009; accepted 8 September 2009
Published online 13 November 2009 in Wiley InterScience (www.interscience.wiley.com). DOI 10.1002/jor.21030

ABSTRACT: Mucopolysaccharidosis VII (MPS VII) is a lysosomal storage disorder characterized by a deficiency in β-glucuronidase activity, leading to systemic accumulation of poorly degraded glycosaminoglycans (GAG). Along with other morbidities, MPS VII is associated with pediatric spinal deformity. The objective of this study was to examine potential associations between abnormal lumbar spine matrix structure and composition in MPS VII, and spine segment and tissue-level mechanical properties, using a naturally occurring canine model with a similar clinical phenotype to the human form of the disorder. Segments from juvenile MPS VII and unaffected dogs were allocated to: radiography, gross morphology, histology, biochemistry, and mechanical testing. MPS VII spines had radiolucent lesions in the vertebral body epiphyses. Histologically, this corresponded to a GAG-rich cartilaginous region in place of bone and elevated GAG staining was seen in the annulus fibrosus. Biochemically, MPS VII samples had elevated GAG in the outer annulus fibrosus and epiphyses, low calcium in the epiphyses, and high water content in all regions except the nucleus pulposus. MPS VII spine segments had higher range of motion and lower stiffness than controls. Endplate indentation stiffness and failure loads were significantly lower in MPS VII samples, while annulus fibrosus tensile mechanical properties were normal. Vertebral body lesions in MPS VII spines suggest a failure to convert cartilage to bone during development. Low stiffness in these regions likely contributes to mechanical weakness in motion segments and is a potential factor in the progression of spinal deformity. J Orthop Res 28:616–622, 2010

Keywords: lumbar spine; mucopolysaccharidosis VII; mechanical properties; spinal deformity

Mucopolysaccharidosis VII (MPS VII), or Sly Syndrome, is a rare, hereditary lysosomal storage disorder characterized by a deficiency in β-glucuronidase activity, leading to the systemic accumulation of poorly degraded chondroitin, dermatan, and heparan sulfate glycosaminoglycans (GAG).[1,2] Clinically, signs of the disease include physical deformity and impeded mental development. Patients typically have a reduced life span. In the spine, the disease is characterized by poorly formed and aligned vertebral bodies, which has been associated with high incidences of kyphosis and scoliosis.[1,3,4]

In MPS VII, long bones are shortened and thickened [5] and contain radiolucent lesions in the epiphyses.[6] Recent research demonstrated increased lumbar intervertebral disc height associated with MPS VII, potentially indicative of similar pathology.[2] Beyond these radiographic observations, however, the etiologies of spinal deformities from structural and biomechanical perspectives have not been described. Their elucidation would enable interventional biological or surgical treatments to be targeted with respect to both anatomical location and the developmental stage of the patient.

Established animal models of MPS VII include mutant mouse models[7–9] and naturally occurring canine[2,10] and feline[11,12] models, each of which exhibit similar pathological characteristics to the human form of the disorder.[13] Our objective was to investigate the consequences of MPS VII for the structure, composition, and mechanical properties of skeletally immature lumbar spines, as possible foundations for spinal deformities, using a naturally occurring canine model. The large size of this model facilitated analyses of regional biochemical composition and tissue level mechanical properties. Furthermore, large animal homologues such as dogs show similarities to humans with regard to natural genetic diversity, facilitate similar approaches to therapy and care, and allow the evaluation of long-term effects of treatment.[14] We hypothesized that abnormal matrix structure and biochemical composition associated with impaired cell function in MPS VII would result in altered spine segment stiffness and range of motion, and, at the tissue level, in altered annulus fibrosus (AF) and vertebral body endplate mechanical properties.

MATERIALS AND METHODS

Specimen Preparation

Animals were raised at the School of Veterinary Medicine at the University of Pennsylvania, under NIH and USDA guidelines for the care and use of animals in research. With institutional IACUC approval, lumbar spines were obtained post-mortem from four MPS VII-affected juvenile dogs and four healthy dogs as controls (age = 5.7 ± 0.3 months, mean ± SD). As in humans, MPS VII in dogs is inherited as an autosomal recessive trait. The affected animals were from a breeding colony originally established from a single heterozygous animal. Two of the control animals were from the same family as the affected animals; the other two were unrelated animals of similar size and weight. Six bone–disc–bone spine motion segments from T12 to L7 were isolated, and zygapophyseal joints were removed and discarded. Those for biomechanical, radiographical, and biochemical experiments were frozen until testing; those for gross morphology and histology were placed in buffered 10% formalin.

Correspondence to: Dawn M. Elliott (T: 215-898-5583; F: 215-573-2133; E-mail: delliott@mail.med.upenn.edu)

Histology

Following fixation, L2–3 segments were decalcified and a 5 mm-thick, midsagittal slab was removed, photographed for gross morphological examination, and processed for paraffin histology. Ten-micron sections were double stained with alcian blue and picrosirius red to demonstrate GAG and collagen distribution, respectively. The AF, nucleus pulposus (NP), and vertebral body epiphyses were examined using bright field light microscopy.

Spine Motion Segment Mechanical Testing

Spine motion segments (L1–2) were thawed and lateral radiographs taken using a fluoroscope (Hologic, Bedford, MA, USA). Vertebral bodies were potted in custom aluminum cups using alignment screws, PMMA, and K-wires. Following overnight equilibration in phosphate-buffered saline (PBS), samples were tested in 20 tension–compression loading cycles (to dissipate hyperswelling effects[15]) between 45 N and −90 N (Instron, Norwood, MA, USA) at a rate of 0.3 mm/s, followed by a creep test (1-s step load from zero to −90 N held for 1 h). The maximum compressive load of −90 N was selected to apply a 0.48-MPa stress, which corresponds to the stress in a human disc under one body weight.[16] Samples were then cut midaxially through the disc and photographed; total area was determined from the image using a custom written program, in which the disc perimeter was manually traced and the included area calculated from a binary mask [17] (Matlab V7; Mathworks, Natick, MA, USA). Compressive and neutral zone stiffness, total range of motion, and creep displacement were calculated.[16]

Vertebral Body Endplate Indentation Testing

The inferior vertebral body, flensed of soft tissue, was mounted face up in an aluminum cup using alignment screws, fixed in position using PMMA, and mounted in the PBS testing bath. A 1.5 mm-diameter spherical tip was used to indent each sample at 0.2 mm/s in the central, anterior, and lateral regions (Fig. 1A). The results of one indentation test were excluded as the tip slipped off the edge of the vertebral rim. Failure load (the peak load reached during the test) and failure displacement were calculated. To calculate linear region stiffness, a sixth-order polynomial was fitted to the load-displacement data up to the failure load; stiffness was then calculated as the maximum of its first derivative.

Annulus Fibrosus Tensile Mechanical Testing

Intervertebral discs (L4–5 or L5–6) were separated from adjacent vertebral bodies at the end plates using a scalpel. A circumferentially oriented strip was removed from the anterior AF (Fig. 1B), equilibrated for 1 h in PBS at 4°C, and trimmed to a uniform thickness using a freezing stage microtome. Specimen cross-sectional area was then measured using a custom laser device.[18] The surface was speckle-coated with India ink, and the specimen was mounted in the mechanical testing system and submerged in PBS. Following the application of a 0.1 N tare load, the specimen was preconditioned for 10 cycles to 5% strain followed immediately by a quasi-static ramp test at a rate of 0.01 %/s. Surface images were analyzed to determine axial tissue strain (Vic-2D; Correlated Solutions, Columbia, SC, USA). Linear and toe region elastic moduli and transition strain were determined using a bilinear fit.[19]

Differences in the mechanical properties of motion segments, endplates, and the AF between MPS VII and unaffected samples were examined using unpaired Student's *t*-tests. Regional variations in endplate indentation properties in affected and unaffected samples were examined using one-way analysis of variance (ANOVAs) followed by Tukey pairwise post hoc tests. All statistical tests were performed using GraphPad Prism 5 (GraphPad Software; La Jolla, CA, USA).

Region Biochemical Composition

Intervertebral discs were removed at the endplates from L5–6 or L6–7 spine segments using a scalpel. Disc tissue samples were dissected from the NP, inner anterior AF, and outer anterior AF. Anterior, inferior epiphysis samples were obtained as follows: all cartilage was carefully cleaned from the endplate surface, and parallel incisions were made to the depth of the growth plate followed by an incision parallel to the growth plate. Samples were then divided into two equal portions. All specimens were weighed to determine wet weight, dried overnight at 60°C, and reweighed to determine dry weight and water content. AF, NP, and one epiphysis sample were then digested using proteinase K. Sulfated GAG was

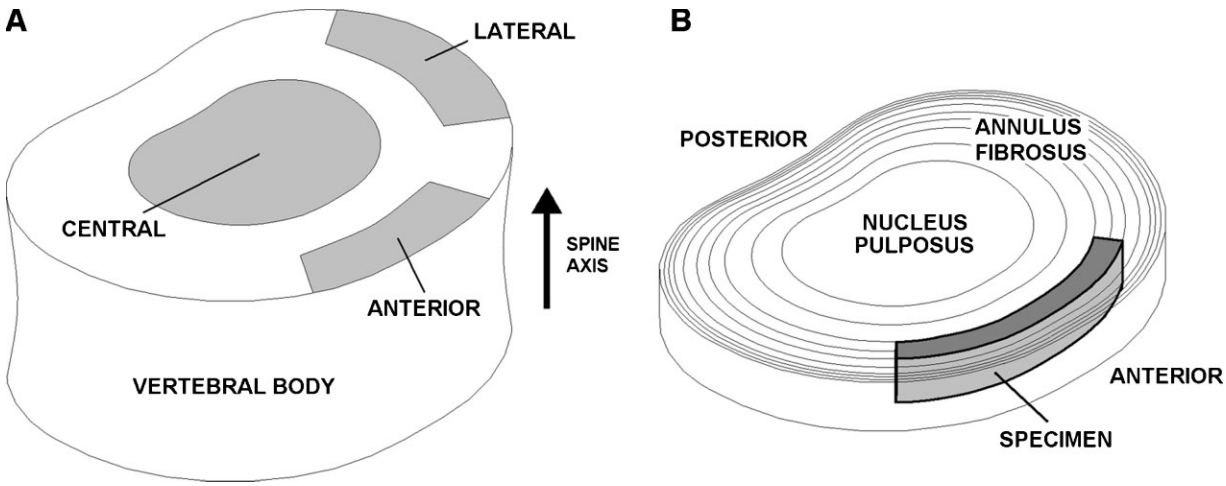

Figure 1. (A) Vertebral body schematic showing central, anterior, and lateral sites for end plate indentation testing. (B) Intervertebral disc schematic showing the specimen excision site for AF tensile testing.

measured using the dimethylmethylene blue assay.[20] The second endplate sample was incubated overnight in 0.5 M HCl; total calcium content was then measured using the *o*-cresolphthalein complexone technique.[21] Measured constituents were normalized by sample dry weight. Differences in biochemical composition in each region between MPS VII and unaffected samples were assessed using unpaired Student's *t*-tests. Regional variations in biochemical properties in affected and unaffected samples were examined using one-way ANOVAs followed by Tukey pair-wise post hoc tests.

RESULTS

Structural Observations

Marked differences were observed in the structure of MPS VII spines compared to unaffected spines (Fig. 2). Lateral fluoroscope images (Fig. 2A and B) showed radiolucent lesions in MPS VII samples anteriorly and posteriorly, immediately adjacent to the intervertebral disc; no such lesions were observed in unaffected samples. Gross morphology (Fig. 2C and D) showed a white homogeneous material in the peripheral regions of the epiphyses in MPS VII samples associated with these lesions, in place of trabecular bone. Alcian blue-picrosirius red stained sections (Fig. 2E and F) showed elevated GAG staining associated with these epiphyseal lesions in MPS VII samples, and high GAG staining throughout the AF of the disc relative to unaffected samples. Closer examination (Fig. 3) revealed that in MPS VII samples, epiphyseal lesions were composed of a GAG-rich, cellular cartilaginous material in place of trabecular bone (Fig. 3A–D), and significant GAG infiltration into the lamellae of the AF relative to unaffected samples (Fig. 3E–H).

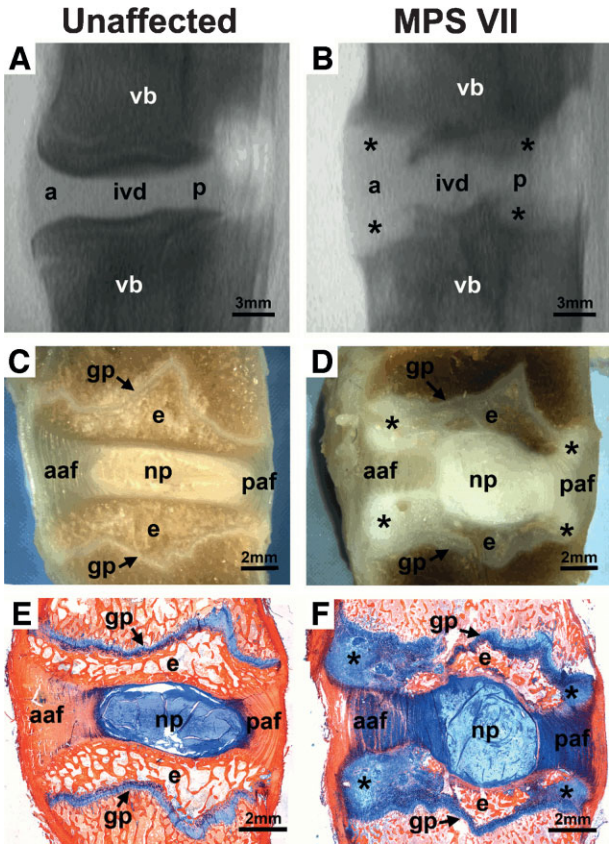

Figure 2. Structural comparisons of unaffected and MPS VII lumbar spine segments (ivd = intervertebral disc; vb = vertebral body; a = anterior; p = posterior; aaf = anterior AF; paf = posterior AF; np = nucleus pulposus; e = epiphysis; gp = growth plate). (A) Lateral radiograph of an unaffected spine segment. (B) Lateral radiograph of MPS VII spine segment showing radiolucent lesions (*) in the vertebral bodies. (C) Gross morphology of an unaffected spine segment (midsagittal section). (D) Gross morphology of an MPS VII spine segment (midsagittal section) showing lesions (*) localized to the peripheral epiphyses. (E) Alcian blue-picorsirius red stained section from an unaffected spine segment. (F) Alcian blue-picorsirius red stained section from an MPS VII spine segment showing high GAG staining (blue) in epiphyseal lesions (*) and throughout the AF.

Mechanical Properties

No significant difference in disc area was found between MPS VII and unaffected samples. Motion segment mechanical testing results for unaffected samples were comparable to those reported previously.[22] Compressive and neutral zone stiffness were both significantly lower for MPS VII motion segments compared to unaffected segments (Fig. 4A and B; 66 and 19% of unaffected, respectively, both $p < 0.05$). Total range of motion was significantly greater for MPS VII samples (Fig. 4C; +216% of unaffected, $p < 0.05$). Creep displacement was significantly greater for MPS VII samples (Fig. 4D; +194% of unaffected $p < 0.05$). Endplate indentation properties of unaffected samples were comparable to those reported previously for the human vertebral endplate.[23] Stiffness in unaffected samples was not significantly affected by region. For MPS VII samples, the stiffness in the anterior region showed a trend to be lower than for other regions ($p = 0.07$). Comparing unaffected and MPS VII samples, the latter were significantly less stiff in all three regions (Fig. 5A; central: 50% of unaffected, $p < 0.005$; anterior: 24% of unaffected, $p < 0.05$; and lateral: 30.4% of unaffected, $p < 0.005$). Like stiffness, failure load did not have significant regional dependence. Failure load was significantly lower in MPS VII samples (Fig. 5B, central: 51% of unaffected, $p < 0.05$; anterior: 18% of unaffected, $p < 0.05$; and lateral: 35% of unaffected, $p < 0.005$). Failure displacement was not significantly different between regions in either group, and no differences were found between MPS VII and unaffected samples in any region (Fig. 5C). AF sample cross-sectional area was 2.1 ± 0.61 mm^2. AF tensile mechanical properties (Fig. 6) were of similar magnitude to those reported previously for human tissue.[24,25] No tensile properties were significantly different between MPS VII and unaffected samples.

Regional Biochemical Composition

In unaffected samples, significant differences were found in water and GAG content between all regions ($p < 0.05$). In MPS VII samples, there were no significant regional differences in water content, with GAG content significantly different only between the NP and

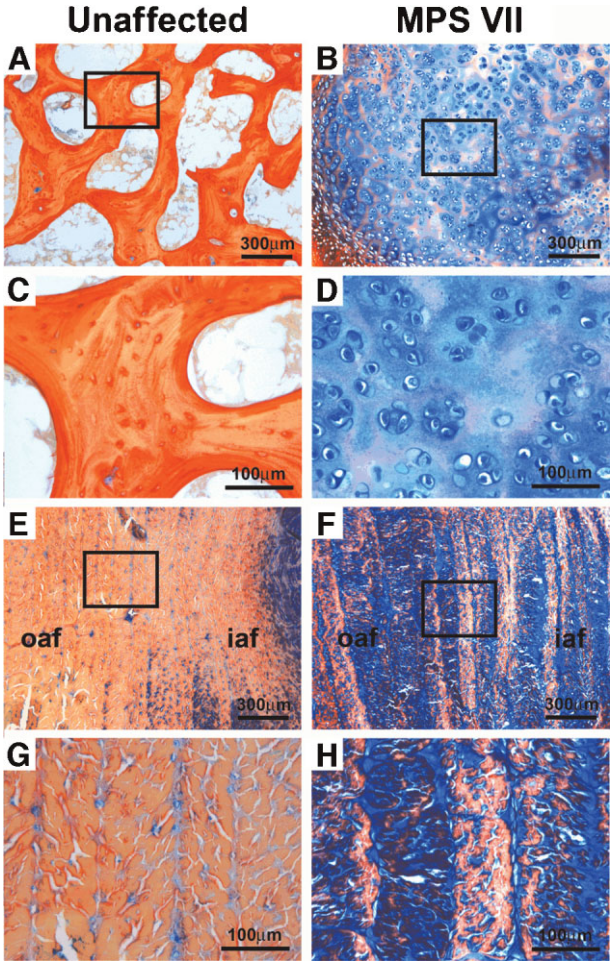

Figure 3. High magnification images of alcian blue-picrosirius red stained sections illustrating structural and compositional differences in the AF and anterior epiphyses between MPS VII and unaffected samples. (A) Anterior epiphysis of an unaffected sample containing trabecular bone. (B) Similar region in an MPS VII sample showing cellular cartilaginous material with high GAG content (blue). (C, D) Higher magnification views of insets indicated in A and B, respectively. (E) Anterior AF of an unaffected sample. (F) Similar region in an MPS VII sample showing elevated GAG staining within annulus lamellae. (G, H) Higher magnification views of insets indicated in E and F, respectively.

epiphysis ($p < 0.05$). In MPS VII samples, water content was significantly higher than in unaffected samples in all regions except the NP (Fig. 7A, inner AF: 109% of unaffected, $p < 0.05$; outer AF: 124% and epiphysis: 225% of unaffected, both $p < 0.005$). GAG content was significantly higher for MPS VII samples in the outer AF and epiphysis (Fig. 7B, 194 and 783% of unaffected, respectively, both $p < 0.005$), but not in the inner AF or NP. Calcium content in the anterior epiphysis of MPS VII samples was 46% of that measured in unaffected samples (Fig. 7C, $p < 0.005$).

DISCUSSION

Although spinal deformity is an established clinical sign of MPS VII, the potential roles of altered lumbar spine segment structure, composition, and mechanical properties in its progression have not been characterized. We examined these parameters comprehensively using a canine model. Radiolucent lesions, similar to those noted previously in the spine and long bones,[2,6] were observed, and their histological appearance was described. Apparent high GAG content and low mineral content in these regions was confirmed biochemically. These findings may be indicative of a failure of epiphyseal cartilage to convert to mineralized bone during development, and are consistent with previous suggestions that lysosomal accumulation inside osteoblasts, osteocytes, and chondrocytes in MPS VII, particularly those of the growth plate, impedes the ability of these cells to regulate cartilage and bone formation and remodelling.[26] Significantly reduced vertebral body endplate stiffness and failure load are most likely attributable to abnormal composition associated with these lesions (elevated GAG and water content, and absence of mineral), and likely contribute to the decrease in motion segment stiffness and increased range of motion. Mechanical weakness in anterior and lateral regions, in particular, may contribute to the progressive onset of kyphotic and scoliotic deformity, respectively. Increased creep displacement of MPS VII-affected spine segments may be attributable to increased deformations in the disc and uncalcified regions of the vertebral epiphyses, as both these tissues exhibited altered composition and structure with the pathology.

The AF performs multiple important mechanical roles in the intervertebral disc, including facilitating joint mobility and generating circumferential hoop stresses under compressive loads. Altered AF mechanical properties as a consequence of altered microstructure or composition would have significant consequences for mechanical behavior of the spine. Other musculoskeletal

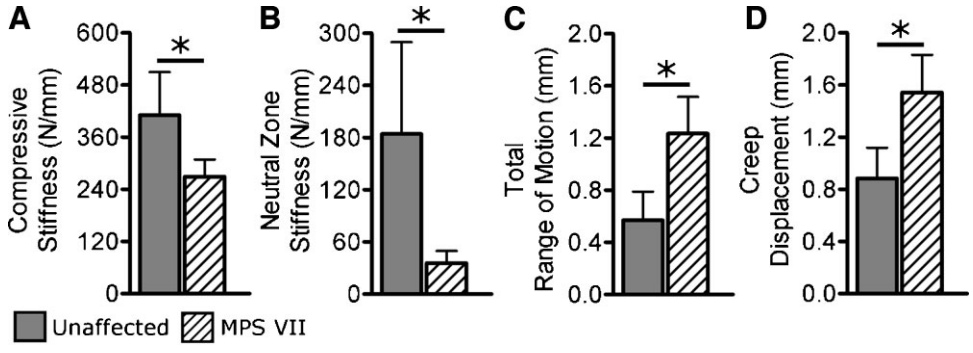

Figure 4. Spine motion segment mechanical testing results. (A) Compressive stiffness was significantly lower for MPS VII samples. (B) Neutral zone stiffness was also significantly lower for MPS VII samples. (C) Total range of motion was greater for MPS VII samples. (E) Creep displacement was significantly greater for MPS VII samples. Mean ± SD, $^*p < 0.05$.

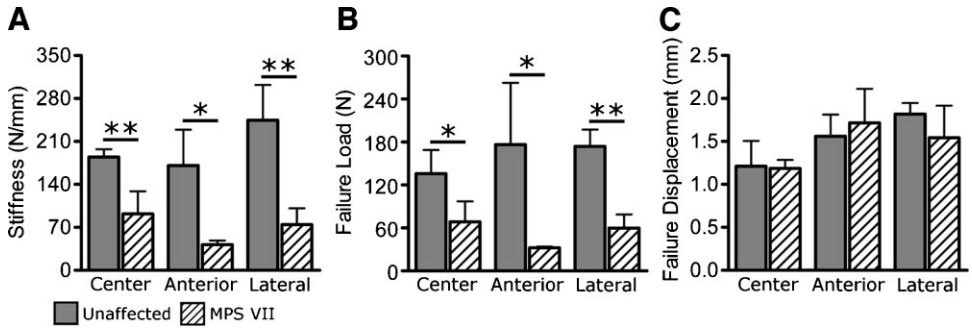

Figure 5. Vertebral body endplate indentation testing results. (A) Stiffness. (B) Failure load. Both properties were significantly lower for MPS VII samples in all regions. (C) Failure displacement was not significantly different in any region. Mean ± SD, $^{*}p < 0.05$, $^{**}p < 0.005$.

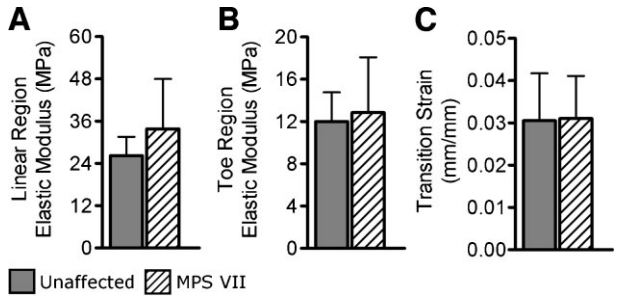

Figure 6. AF circumferential tensile mechanical testing results. (A) Linear region elastic modulus. (B) Toe region elastic modulus. (C) Transition strain. None of these properties were significantly different between groups. Mean ± SD.

tissues show increased activity of inflammatory proteases including the MMPs -2 and -9 (gelatinases) and MMP-13 (a collagenase) as a consequence of MPS VII.[10,13] In this study, AF tensile properties, both in the toe region where collagen fibers are realigning and uncrimping and in the linear region where fibers are fully engaged, were not significantly different for MPS VII samples compared with controls, suggesting that any alterations in collagen fibril morphology as a result of increased activity of these catabolic factors have minimal functional consequence.

In the epiphyses, increased water content is likely due to both elevated GAG and the presence of uncalcified cartilage in place of mineralized bone. In the AF, increased water content is most likely a direct result of increased GAG content. Interestingly, tensile properties were not found to be significantly affected by the pathology, suggesting that increased GAG and water content do not significantly disrupt fiber load bearing capacity. Recent research demonstrated a positive correlation between outer AF ultimate tensile strength and vertebral body yield strength,[27] highlighting the functional interrelationships that exist between these two structures. In our study, weakened vertebral endplate mechanics in MPS VII were not accompanied by a concomitant decrease in AF mechanical properties. Abnormal GAG accumulation and associated increased hydration within the AF lamellar structure may act to protect the AF from mechanically induced degeneration. Examination of older animals would confirm this.

Developmental differences exist between canine and human skeletons, including the nature of secondary ossification in the vertebral bodies, which may affect the pathogenesis of bone lesions. In humans, vertebral secondary ossification centers are relatively small and U-shaped, and do not form until the onset of puberty.[28] Developmentally, the age of the animals in our study corresponds to early adolescence in humans. Underdevelopment of the inferior and superior regions of the lumbar and thoracic vertebral bodies was reported in an MPS VII patient aged just 2 months, suggesting the presence of lesions precedes secondary ossification.[1] Associated kyphosis and scoliosis was noted at 2 years of age.[1] If lesions are left untreated, when patients reach adolescence, the rapid period of skeletal growth would likely result in further substantial spinal deformity.

Zygapophyseal joints were removed to facilitate more direct assessment of the mechanical contributions of the intervertebral disc and vertebral bodies. The potential contribution of these joints, and associated muscles and ligaments, to altered mechanical properties and progression of deformity, cannot be discounted, and should be the subject of future studies.

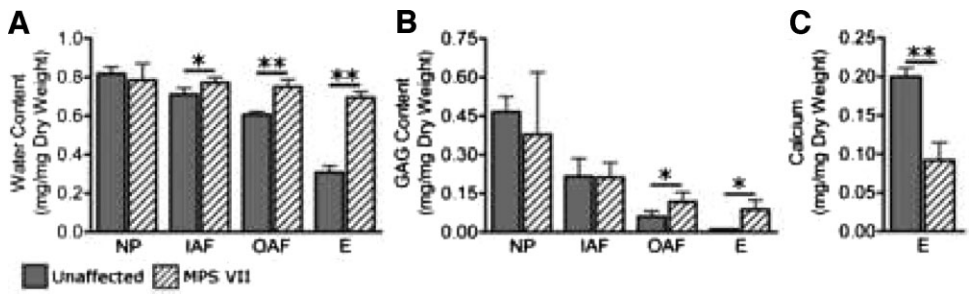

Figure 7. Comparison of biochemical properties between unaffected and MPS VII samples in the nucleus pulposus (NP), inner AF (IAF), outer AF (OAF), and anterior epiphysis (E). (A) Water content was significantly higher for MPS VII samples in all regions except the nucleus pulposus. (B) GAG content was significantly higher for MPS VII samples in the outer AF and epiphysis. (C) Calcium content was significantly lower in the anterior epiphysis of MPS VII samples. Mean ± SD, $^{*}p < 0.05$, $^{**}p < 0.005$.

Our spine motion segment mechanical properties were not normalized to account for possible differences in disc geometry. Although we were able to demonstrate no significant differences in axial disc area for these segments, attempts to compare disc height prior to testing using lateral radiographs failed, as the presence of radiolucent lesions in MPS VII samples (Fig. 2B) made it impossible to calculate disc height with any degree of accuracy.

Determining mechanisms for ameliorating or reversing the rapid and substantive physical deterioration of the musculoskeletal system associated with MPS VII may result in a significant improvement in the quality of life for patients, in terms of alleviating physical discomfort and improving mobility. Our results show that alterations in motion segment and tissue level mechanical properties can be attributed in part to the apparent failure of mineralized bone to form at the peripheral regions of the vertebral bodies. These results suggest that, in addition to biological therapies, such as enzyme replacement therapy, gene therapy, and hematopoietic stem cell transplantation,[29–31] which have been proposed for systemic treatment of the disease, localized delivery of osteoinductive anabolic factors, such as bone morphogenetic proteins,[32] to these regions may be an effective means of limiting the progression of deformity.

ACKNOWLEDGMENTS

This study was funded by grants from NIH (DK54481, RR02512) and the Penn Center for Musculoskeletal Disorders. The authors thank Patricia O'Donnell, Steven Fernandez, and Dr. Cynthia O'Connor for animal care.

REFERENCES

1. Sly WS, Quinton BA, McAlister WH, et al. 1973. Beta glucuronidase deficiency: report of clinical, radiologic, and biochemical features of a new mucopolysaccharidosis. J Pediatr 82:249–257.
2. Herati RS, Knox VW, O'Donnell P, et al. 2008. Radiographic evaluation of bones and joints in mucopolysaccharidosis I and VII dogs after neonatal gene therapy. Mol Genet Metab 95:142–151.
3. Beaudet AL, DiFerrante NM, Ferry GD, et al. 1975. Variation in the phenotypic expression of beta-glucuronidase deficiency. J Pediatr 86:388–394.
4. Vogler C, Levy B, Kyle JW, et al. 1994. Mucopolysaccharidosis VII: postmortem biochemical and pathological findings in a young adult with beta-glucuronidase deficiency. Mod Pathol 7:132–137.
5. Vogler C, Birkenmeier EH, Sly WS, et al. 1990. A murine model of mucopolysaccharidosis VII. Gross and microscopic findings in beta-glucuronidase-deficient mice. Am J Pathol 136:207–217.
6. Haskins ME, Desnick RJ, DiFerrante N, et al. 1984. Beta-glucuronidase deficiency in a dog: a model of human mucopolysaccharidosis VII. Pediatr Res 18:980–984.
7. Vogler C, Levy B, Galvin N, et al. 2005. Early onset of lysosomal storage disease in a murine model of mucopolysaccharidosis type VII: undegraded substrate accumulates in many tissues in the fetus and very young MPS VII mouse. Pediatr Dev Pathol 8:453–462.
8. Donsante A, Levy B, Vogler C, et al. 2007. Clinical response to persistent, low-level beta-glucuronidase expression in the murine model of mucopolysaccharidosis type VII. J Inherit Metab Dis 30:227–238.
9. Birkenmeier EH, Davisson MT, Beamer WG, et al. 1989. Murine mucopolysaccharidosis type VII. Characterization of a mouse with beta-glucuronidase deficiency. J Clin Invest 83:1258–1266.
10. Simonaro CM, D'Angelo M, He X, et al. 2008. Mechanism of glycosaminoglycan-mediated bone and joint disease: implications for the mucopolysaccharidoses and other connective tissue diseases. Am J Pathol 172:112–122.
11. Gitzelmann R, Bosshard NU, Superti-Furga A, et al. 1994. Feline mucopolysaccharidosis VII due to beta-glucuronidase deficiency. Vet Pathol 31:435–443.
12. Fyfe JC, Kurzhals RL, Lassaline ME, et al. 1999. Molecular basis of feline beta-glucuronidase deficiency: an animal model of mucopolysaccharidosis VII. Genomics 58:121–128.
13. Simonaro CM, D'Angelo M, Haskins ME, et al. 2005. Joint and bone disease in mucopolysaccharidoses VI and VII: identification of new therapeutic targets and biomarkers using animal models. Pediatr Res 57:701–707.
14. Haskins M, Casal M, Ellinwood NM, et al. 2002. Animal models for mucopolysaccharidoses and their clinical relevance. Acta Paediatr Suppl 91:88–97.
15. Johannessen W, Vresilovic EJ, Wright AC, et al. 2004. Intervertebral disc mechanics are restored following cyclic loading and unloaded recovery. Ann Biomed Eng 32:70–76.
16. Beckstein JC, Sen S, Schaer TP, et al. 2008. Comparison of animal discs used in disc research to human lumbar disc: axial compression mechanics and glycosaminoglycan content. Spine 33:E166–E173.
17. O'Connell GD, Vresilovic EJ, Elliott DM. 2007. Comparison of animals used in disc research to human lumbar disc geometry. Spine 32:328–333.
18. Ansorge HL, Beredjiklian PK, Soslowsky LJ. 2009. CD44 deficiency improves healing tendon mechanics and increases matrix and cytokine expression in a mouse patellar tendon injury model. J Orthop Res 10:1386–1391.
19. Lynch HA, Johannessen W, Wu JP, et al. 2003. Effect of fiber orientation and strain rate on the nonlinear uniaxial tensile material properties of tendon. J Biomech Eng 125: 726–731.
20. Farndale RW, Buttle DJ, Barrett AJ. 1986. Improved quantitation and discrimination of sulphated glycosaminoglycans by use of dimethylmethylene blue. Biochim Biophys Acta 883:173–177.
21. Sarkar BC, Chauhan UP. 1967. A new method for determining micro quantities of calcium in biological materials. Anal Biochem 20:155–166.
22. Zimmerman MC, Vuono-Hawkins M, Parsons JR, et al. 1992. The mechanical properties of the canine lumbar disc and motion segment. Spine 17:213–220.
23. Oxland TR, Grant JP, Dvorak MF, et al. 2003. Effects of endplate removal on the structural properties of the lower lumbar vertebral bodies. Spine 28:771–777.
24. Acaroglu ER, Iatridis JC, Setton LA, et al. 1995. Degeneration and aging affect the tensile behavior of human lumbar anulus fibrosus. Spine 20:2690–2701.
25. Ebara S, Iatridis JC, Setton LA, et al. 1996. Tensile properties of nondegenerate human lumbar anulus fibrosus. Spine 21:452–461.
26. Mango RL, Xu L, Sands MS, et al. 2004. Neonatal retroviral vector-mediated hepatic gene therapy reduces bone, joint, and cartilage disease in mucopolysaccharidosis VII mice and dogs. Mol Genet Metab 82:4–19.
27. Skrzypiec D, Tarala M, Pollintine P, et al. 2007. When are intervertebral discs stronger than their adjacent vertebrae? Spine 32:2455–2461.

28. Albert AM, Maples WR. 1995. Stages of epiphyseal union for thoracic and lumbar vertebral centra as a method of age determination for teenage and young adult skeletons. J Forensic Sci 40:623–633.
29. Sly WS. 2004. Enzyme replacement therapy for lysosomal storage disorders: successful transition from concept to clinical practice. MO Med 101:100–104.
30. Ponder KP, Haskins ME. 2007. Gene therapy for mucopolysaccharidosis. Expert Opin Biol Ther 7:1333–1345.
31. Krivit W. 2004. Allogeneic stem cell transplantation for the treatment of lysosomal and peroxisomal metabolic diseases. Springer Semin Immunopathol 26:119–132.
32. Leboy PS. 2006. Regulating bone growth and development with bone morphogenetic proteins. Ann N Y Acad Sci 1068: 14–18.